end of the system without distortion. It is important to make sure the controller in a teleoperation system is designed such that high transparency is achieved. This will ensure that the human operator can perform a task through a teleoperation system with the same ease and performance that he/she does it in a direct-touch situation. In other words, transparency as a measure of system performance and user task performance go hand in hand. We will use the dynamic range or *Z*-width (Ashrafzadeh, 2007) of the transmitted impedance to the operator to analyze the transparency of a bilateral teleoperation system. A larger *Z*-width corresponds to more realistic feelings of the environments for the operator. It is desirable, therefore, to maximize the *Z*-width of a haptic display.

Digital techniques have liberated control designers from time-consuming analog design. However, this means some of the advantages of analog control have been lost (Hewitson, 2010; Brezovich, 2011; Malcher & Falkowski, 2014; Colgate & Brown, 1994), which may have significant performance and stability consequences. This article studies whether a Field Programmable Analog Arrays (FPAA)-based controller can achieve better user task performance compared to a digital controller in bilateral teleoperation.

Due to the discrete interface (ZOH interface), the discrete-time controllers are capable of generating energy; therefore, lower gains must be selected to make the generated energy diffusible through the intrinsic dissipative mechanical components, which may not be acceptable for bilateral teleoperation systems which need high control gain and high system stability at the same time. Thus this article proposes FPAA-based analog controller to eliminate discretization affect while keeping the design process more simple and revisable.

As will be discussed in Section 3, a larger control gain generally leads to a higher teleoperation system transparency and, therefore, improves user task performance. However, when the teleoperation controller is implemented in discrete time, the product of control gain and sampling period is upper bounded as a condition for keeping the system stable. In practice, the value of the sampling period is lower bounded because of the time required for A/D and D/A conversion and the control law implementation, thus resulting in an upper bound on the control gain as far as stability is concerned. A major difficulty arises if this stability-imposed upper bound on the control gain constrains the teleoperation transparency to the level that tasks cannot be completed successfully by the human operator.

One way of solving the aforementioned dilemma is to use fast-sampling processors that provide very small sampling periods such as the field programmable gate array (FPGA) (Liu, Chen, & Wang, 2011; Courtecuisse, Jung, Allard, Duriez, Lee, & Cotin, 2010; Mafi, Sirouspour, Mahdavikhah, Moody, Elizeh, & Kinsman, 2010; Spinner, Srinivasan, & Rengaswamy, 2014). This option will be more expensive than the ubiquitous personal computers, and only shortens the sampling period but does not eliminate the trade-off between the control gain and sampling period fundamentally.

A more affordable way proposed in this article is to use analog components to implement the teleoperation controller. As the analog control system does not sample data, it fundamentally eliminates the limitation brought by the sampling period. This article discusses whether a bilateral teleoperation system with a FPAA-based controller can accomplish tasks requiring high positioning precision (high transparency) and thus high-gain control, while maintaining the system stability.

FPAA is a new type of reconfigurable analog circuits. There are a few vendors that deliver commercially available FPAA circuits, while there are several more FPAA families the production of which has been discontinued, such as the family from Lattice Semiconductor (Ramsden, 2001), the TRAC family from Zetex Semiconductors (Zetex Semiconductors Ltd., 1999), and the MPAA020 from Motorola (Bratt, 1998). One widely used family, still in production, is the PSoC family from Cypress Semiconductor (Cypress Semiconductor Corp., 2014), which is mainly composed of 12 configurable blocks, each of which has to be parameterized and switched on by software. Another popular family is offered by Anadigm with a full range of *5 V* and 3.3 *V* programmable analog arrays (Anadigm Inc., 2004).

Among these commercially available devices, the programmable analog arrays from the Anadigm Company are the most popular circuits (Malcher & Falkowski, 2014). In our work, a dpASP device (second generation

of FPAA) AN231E04 from Anadigm based on switched capacitor technology was used. The AnadigmDesigner2 software provides a simple design template for PID control (Anadigm Inc., 2004).

This article discusses whether a bilateral teleoperation system with an FPAA controller cannot only accomplish tasks that require low control gains, which can be achieved by a digital controller, but also tasks requiring high positioning precision (high transparency), which require high-gain control, while maintaining the system stability.The contribution of this article is in showing that an FPAA-based controller can significantly increase the teleoperation system transparency when compared to its discrete-time counterpart (i.e., the discretized version of the same controller). This improvement in teleoperation system transparency is shown via a user study to translate to enhanced user task performance for the particular task considered in the article. In this way, the article shows that the root cause of task failure in teleoperation can be control sampling (while the blame is routinely placed on ubiquitous non-idealities such as friction, noise, control signal saturation, unmodelled dynamics, communication channel delay, etc., but not on sampling). The continuous-time FPAA-based controller provides these benefits without endangering the system stability. Another contribution of the article is in providing a systematic design approach for the continuous-time haptic teleoperation controller.

The article is organized as follows. The bilateral teleoperation system used in this article is modelled in Section 2. A detailed discussion of stability and transparency conditions needed in our teleoperation system is presented in Section 3. The experimental teleoperation system and the design differences between the FPAA-based controller and the discrete-time controller are shown in Section 4. Section 5 provides the control design procedure considering the constraints brought upon by the two classes of controllers and the empirical approach for designing the FFPAA-based teleoperation. Then, the experimental performances of the two different teleoperation systems under the free-motion and hard contact conditions are shown, and their corresponding parameters of hybrid matrix are compared in Section 6. In Section 7, the human performance of an object stiffness discrimination task using the FPAA-based controlled and discrete-time controlled teleoperation systems is studied and compared. Lastly, concluding remarks are given in Section 8.

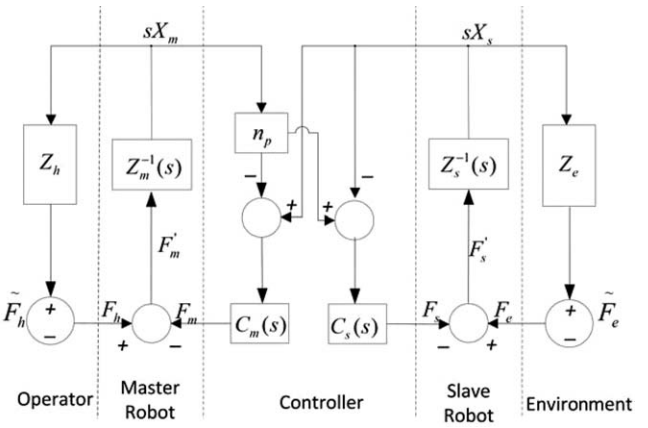

Figure 1. *A continuous-time controlled PEB bilateral teleoperation system.*

2 System Modeling and Control

In this section, the bilateral teleoperation system used in the subsequent sections is modeled. The block diagram of a continuous-time controlled position-error-based (PEB) bilateral teleoperation system is shown in Figure 1, and the corresponding discrete-time PEB teleoperation system is shown in Figure 2. Here, F_h is the interaction force between the master robot and the human operator, and F_e is the interaction force between the slave robot and the environment. Also, F_h and F_e represent the exogenous human operator and environment forces, respectively. X_m and X_s denote the position of the master and slave robots, respectively. Z_h and Z_e are the operator and environment impedances, respectively.

The continuous-time controlled PEB teleoperator in Figure 1 can be modelled in the hybrid matrix form as

$$\begin{bmatrix} F_h(s) \\ -sX_s(s) \end{bmatrix} = H(s) \begin{bmatrix} sX_m(s) \\ F_e(s) \end{bmatrix}, \quad (1)$$

with the following hybrid matrix (Llewellyn, 1952):

$$H(s) = \begin{bmatrix} h_{11} & h_{12} \\ h_{21} & h_{22} \end{bmatrix} = \begin{bmatrix} Z_m + C_m \frac{Z_s}{Z_s+C_s} & \frac{C_m}{Z_s+C_s} \\ -\frac{C_s}{Z_s+C_s} & \frac{1}{Z_s+C_s} \end{bmatrix}. \quad (2)$$

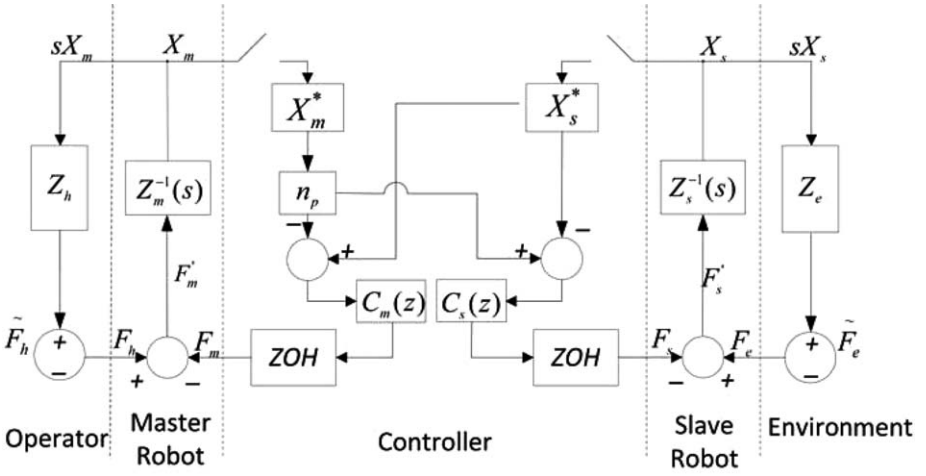

Figure 2. *A discrete-time controlled PEB bilateral teleoperation system.*

In the above, proportional-derivative (PD) position controllers $C_m = k_{v_m}s + k_{p_m}$ and $C_s = k_{v_s}s + k_{p_s}$ are typically used for the master robot and the slave robot, respectively. Given the use of velocities instead of positions in (1), factors of $1/s$ have been introduced in position controllers. In this article, the PEB teleoperation control method is chosen because, for direct force reflection (DFR) control, even a continuous-time controlled teleoperation system will not be absolutely stable (Jazayeri & Tavakoli, 2013). Since the study of the stability–transparency tradeoffs caused by sampling and how they limit task performance is of interest, it is appropriate to start with a known and stable continuous-time teleoperation control architecture, namely the PEB control method.

In Figure 2, the Z_h, Z_e, Z_m, Z_s continue to operate in continuous-time. For the discrete-time controllers, the continuous-time signals X_m and X_s are sampled at time instants separated by T (Ogata, 1995) as

$$X^*(s) = \sum_{k=0}^{\infty} x(kT)e^{-skT}. \tag{3}$$

The z-domain equivalent of (3) is $X(z)=X^*(s)\big|_{s=1/T\ln z}$. The Zero-Order-Hold (ZOH) blocks are used to convert the output of the discrete-time controller to continuous-time with the transfer function

$$G_h(s) = \left(1 - e^{-sT}\right)/sT. \tag{4}$$

The corresponding dynamic models of these two teleoperation systems are shown in the Appendix.

3 Discussion of Stability and Transparency

Details of the stability conditions and transparency of the aforementioned PEB teleoperation system are shown next.

3.1 Transparency of a PEB Teleoperation System

In order to obtain satisfactory system transparency and good user performance, correspondence between the master and slave positions and the master and slave forces is required. This amounts to $H(s)$ being as close to

$$H_{\text{ideal}} = \begin{bmatrix} 0 & 1 \\ -1 & 0 \end{bmatrix} \tag{5}$$

as possible. Evidently, this would happen in (2) if the gains in the controllers C_m and C_s are large enough. However, as it will be shown in Section 3.2, this will pose a problem for stability.

Transparency can be examined from another perspective as well. The impedance perceived by the operator Z_{to} is $(F_h/sX_m)\big|_{\tilde{F}_h=0}$, and the impedance of the environment Z_e is $(F_e/sX_s)\big|_{\tilde{F}_e=0}$. Using (3) and (21) and (23) in the Appendix, we can express Z_{to} in terms of the hybrid parameters and Z_e as

$$Z_{to} = (h_{11} + \Delta h \cdot Z_e)/(1 + h_{22} \cdot Z_e), \tag{6}$$

where $\Delta h = h_{11}h_{22} - h_{12}h_{21}$.

To quantify transparency, Z_{to} is examined for extreme values of Z_e, that is, when the slave is in free motion ($Z_e = 0$) or clamped ($Z_e \to \infty$):

$$\begin{aligned} Z_{to\,\min} &= Z_{to}|_{Z_e=0} = h_{11}, \\ Z_{to\,\max} &= Z_{to}|_{Z_e\to\infty} = \Delta h/h_{22}. \end{aligned} \tag{7}$$

Thus, the ideal values of the hybrid parameters in (5), that is, $h_{11} = h_{22} = 0$ and $h_{12} = -h_{21} = 1$, ensure $|Z_{to\,\min}| \to 0$ and $|Z_{to\,\max}| \to \infty$. This can be used as another way to assess transparency.

3.2 Stability of a PEB Teleoperation System

Having modeled a teleoperation system as a two-port network (teleoperator comprising the master, the controller, and communication channel, and the slave) coupled to two one-port networks (environment and operator) paves the way for ensuring closed-loop stability via teleoperator absolute stability. The absolute stability of a teleoperator is equal to the bounded-input/bound-output stability of the overall teleoperation system assuming that the two one-port terminations are passive but otherwise arbitrary.

A continuous-time absolute stability criterion was proposed by Llewellyn for two-port networks (Llewellyn, 1952; Haykin, 1970), which can be applied to give closed-form conditions involving the teleoperator's immittance (impedance, admittance, hybrid, or transmission) matrix. The PEB teleoperation system of Figure 1 is absolutely stable if k_{pm}, k_{vm}, k_{ps}, $k_{vs} > 0$ and $C_m(s)/C_s(s) = \alpha$, where α is a positive constant (Tavakoli & Aziminejad, 2007).

In the system shown in Figure 2, which is the sampled-data counterpart of the teleoperation system in Figure 1, the PD controllers are discretized, for example, using backward difference method, to

$$\begin{aligned} C_m(z) &= k_{vm}(z-1)/Tz + k_{pm}, \\ C_s(z) &= k_{vs}(z-1)/Tz + k_{ps}. \end{aligned} \tag{8}$$

If $k_{vm} = k_{vs} = k_v$, and $k_{pm} = k_{ps} = k_p$, a sufficient stability condition can be found for the sampled-data teleoperator (Jazayeri & Tavakoli, 2013) as

$$\frac{b_m b_s}{b_s + b_m} > \frac{k_p T}{2} + k_v. \tag{9}$$

For a given teleoperation system, the left side of (9) is fixed. Thus, the stability condition puts an upper bound on k_pT and k_v.

3.3 Analysis of Stability and Transparency Conditions

Based on the above results for the stability and transparency of a PEB teleoperation system, the discrete-time absolute stability condition (9) imposes a trade-off between the sampling period and the proportional gain of the PD controllers. This, combined with the transparency requirements (i.e., high gains in the PD controllers to make [2] approach [5]), show a trade-off between stability and transparency for a fixed sampling period. Indeed, a larger control gain leads to higher transparency but can jeopardize the stability of the sampled-data teleoperation system due to (9). This is in contrast to the continuous-time control case where there is no constraint put on the controller gains by the stability condition, and thus no significant stability-imposed constraint on transparency. These show the significance of comparing the system transparency and the task performance achievable with continuous-time versus discrete-time control.

4 Controller Implementation in a Teleoperation System

This section presents our experimental setup and the differences between discrete-time and continuous-time control in terms of their implementation and design

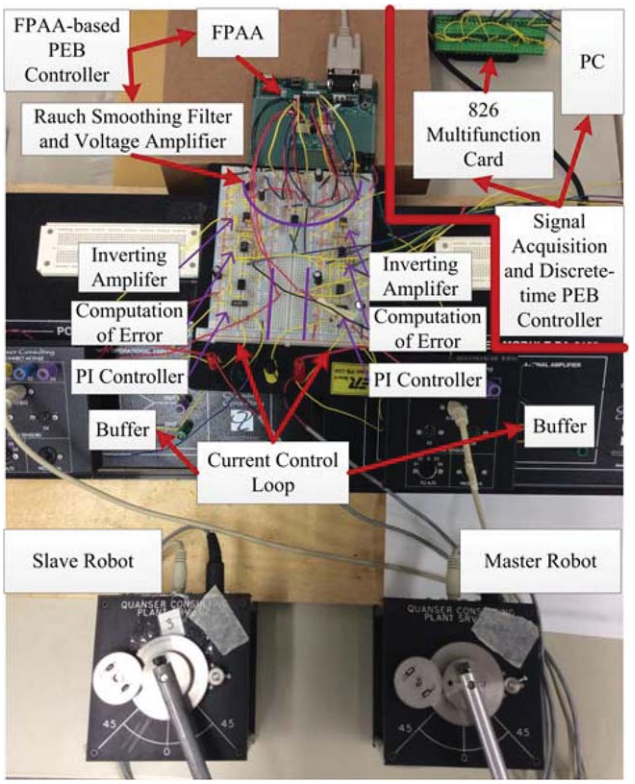

Figure 3. *The experimental setup of the bilateral teleoperation system.*

issues. In both cases, our setup consists of two identical Servo SRV-02 Quick Connect Modules (Quanser Inc., Markham, ON, Canada) as one-degreee-of-freedom, revolute-joint master and slave robots (see Figure 3). Each of the master and slave modules, which is comprised of a DC motor, a gear, and a potentiometer, is preceded by an *inner* current control loop so that an *outer* position control loop can send torque commands (i.e., F_m and F_s in Figure 2) to each robot. While the inner current control loop is always implemented by analog components, the outer-loop position controller can be implemented either in the continuous-time or in the discrete-time domain.

4.1 Current Control Loop

Many commercial robots can be torque-controlled thanks to current control loops integrated inside them. When robots do not have such internal current controllers, as is the case with our setup, there is a need to design a current controller and do so in the continuous time; this is because the response of the current control loop needs to be several times faster than that of the outer position control loop.

A circuit diagram of the analog current control loop implemented for each of the master and slave robots is shown in Figure 4. The input voltage V_{ref} is proportional to and represents the set-point value for the current I_M passing through the motor M. The voltage V_{ref} is fed to the current control circuit (inner control loop) in Figure 4 from the circuit in Figure 5 for the position control loop (outer control loop), which will be discussed later.

In Figure 4's Inverting Amplifier block, a voltage proportional to the negative of the actual motor current is generated: Choice of R_9, R_{10}, R_{11}, and C in the PI Controller block will ensure good rise time in current tracking. The controller output V_{PI} is then fed to the Buffer block so that the commanded V_{ref} representing the desired motor current is compared to V_{IA} representing the actual motor current. Then, the error voltage $V_E = -(V_{ref} + V_{IA})$ is fed to the PI Controller block. Proper choice of R_9, R_{10}, R_{11}, and C in the PI Controller block will ensure good rise time in current tracking. The controller output V_{PI} is then fed to the Buffer block so that the commanded current can be supplied to the motor M. Overall, the loop in Figure 4 will ensure fast and accurate current control for each of the master and slave robots. Knowing the static relationships between current and torque for the DC motors, each of the robots is now torque-controlled.

4.2 Position Control Loop

Having ensured the master and slave robots are torque controlled by using the current control loop in the previous section, the PEB teleoperation control system in Figure 2 needs to be implemented. Whether the position controllers $C_m(s)$ and $C_s(s)$ embedded in this PEB system are implemented in discrete-time (using a PC) or in continuous time (using an FPAA) will lead to two cases. The main difference between discrete-time and the continuous-time control is the use of configurable analog circuits in making the latter.

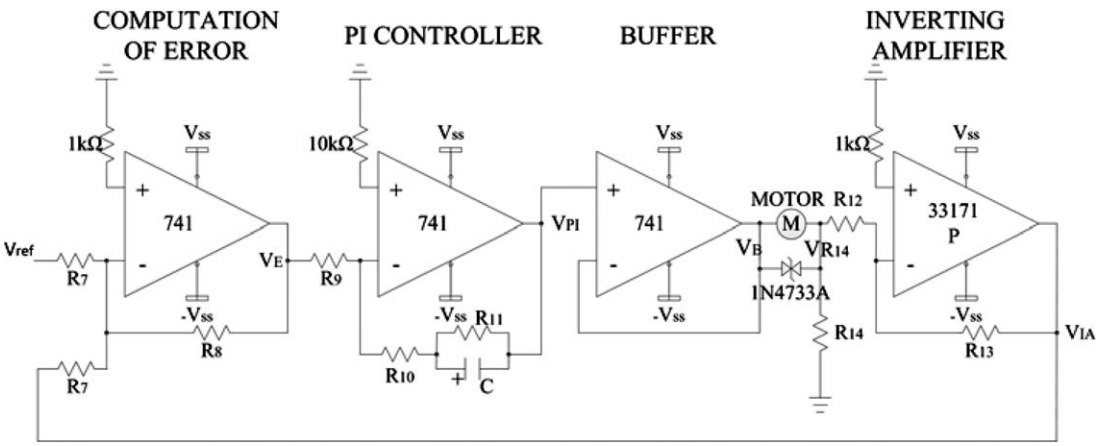

Figure 4. *Circuit diagram of the current control loop.*

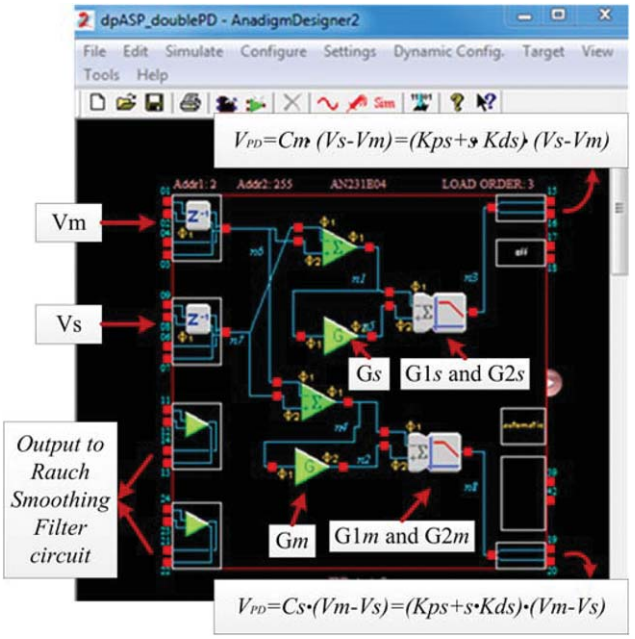

Figure 5. *Circuit realization of a PD controller.*

4.2.1 Discrete-Time Position Control. Digital signals are processed in a PC with a dual-core AMD Opteron Processor 270 at 1.99 GHz with a 64-bit Windows 7 operating system. A Model 826 multifunction analog/digital I/O card (Sensoray Co., Tigard, OR, USA) is used for A/D and D/A conversion. First, the master and slave positions are acquired following A/D conversion of voltages of potentiometers mounted at the robots' joints. Next, the master/slave position error is calculated and fed to the backward-difference discrete-time PD controller in (8) for each of the master and slave robots. Then, following D/A conversion, the control signals F_m and F_s are output to the master and slave robots, respectively. The sampling frequency is 1000 Hz.

4.2.2 FPAA-Based Position Control. While the previous section discussed the implementation of the position controllers needed in the PEB teleoperation control system in Figure 2, this section shows the same but for the control system in Figure 1, which operates entirely in the continuous time.

Figure 5 shows a circuit realization of PD controllers using the AN231E04 FPAA device in the professional design software AnadigmDesigner 2.7.1. Each control circuit is composed of these Configurable Analog Modules (CAM):

- SumDiff CAM: 
- GainHalf CAM: 
- SumFilt CAM: 

The master and slave robots' positions V_m and V_s (i.e., the voltage readouts from the corresponding potentiometers) are inputs to Figure 5 (and Figure 6). For the master robot, in the SumDiff CAM, V_s is added to $-V_m$ (the gains of the inputs in theSumDiff CAM can be chosen

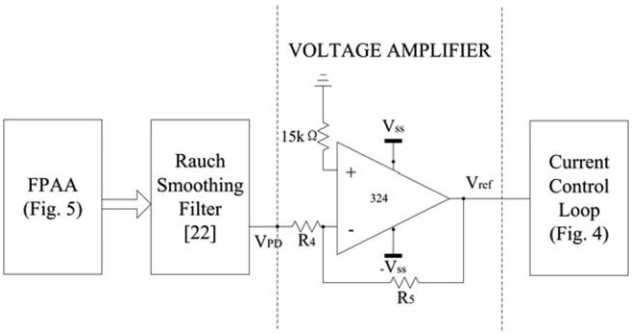

Figure 6. *Circuit diagram of the continuous-time position controller C_m or C_s based on the FPAA in Figure 5.*

differently if position scaling between the master and slave robots is desired). Then, $V_s - V_m$ is input to the GainHalf CAM, which generates a phase-delayed half-cycle gain G to implement the differentiator required as part of the PD control. The proportional control is tuned by changing the gains G_1 and G_2 in the SumFilt CAM. A similar procedure happens on the slave side. Overall, the PD control gains for the master and the slave will be

$$K_{pm} = G_{1m} - G_m \cdot G_{2m}, K_{dm} = (G_m \cdot G_{2m})/F_c,$$
$$K_{ps} = G_{1s} - G_s \cdot G_{2s}, K_{ds} = (G_s \cdot G_{2s})/F_c, \quad (10)$$

respectively, where K_{pm}, K_{ps} are the proportional gains, and K_{dm}, K_{ds} are the differential gains. Here, G_m and G_s are the gains of the GainHalf CAM for the master robot controller and the slave robot controller, respectively, G_{1m} and G_{2m} are the input gains in the SumFilt CAM in the master side, while G_{1s} and G_{2s} are the corresponding constants in the slave side, and F_c is the clock frequency.

These output voltages go through Rauch (also known as multiple feedback) differential filters to smooth the control signals, which later need to be amplified to meet the task requirements.

The PD controller $C_m(s)$ in Figure 1 will now be realized using the circuit shown in Figure 6, and a similar circuit will be used for implementing $C_s(s)$. In Figure 6, V_{PD} represents the voltage output from the FPAA-based PD controller after being filtered, which may be amplified using an op-amp stage. Overall, assuming a unity gain for the Rauch Smoothing Filter block, the master and slave controllers' transfer functions incorporating the PD Controllers in FPAA and the Voltage Amplifier blocks will be

$$C_m = \frac{R_5}{R_4}\left(K_{pm} + s \cdot K_{dm}\right),$$
$$C_s = \frac{R_5}{R_4}\left(K_{ps} + s \cdot K_{ds}\right). \quad (11)$$

5 Method of Designing FPAA-Based Controller in a Teleoperation System

5.1 Constraints in the Design of Controllers in a Teleoperation System

Finding appropriate values of resistors to generate the required control gains needs due attention in the case of analog control implementation. For instance, it is important to avoid saturating the operational amplifiers or overloading the motors while achieving accurate (high-gain) current and position control. In the following, the design constraints for the position control loop are discussed in detail while the constraints for the current control loop, which can be derived in a similar way, are omitted for brevity.

5.1.1 Constraints in the Haptic Teleoperation Position Controller Design for a Single Robot. *Op-amp Saturation Protection*: The following conditions are needed to avoid the saturation of the op-amps in Figure 6 (from left to right, respectively):

$$|V_m| \le V_F,\ |V_s| \le V_F,\ |V_{PD}| \le V_F, \quad (12)$$

$$|V_{PD}| = \left|\left(K_p + s \cdot K_d\right) \cdot (V_s - V_m)\right|, \quad (13)$$

$$\max\left(\left|V_{ref}\right|\right) \le V_{ss},$$
$$\left|V_{ref}\right| = \left|\frac{R_5}{R_4} V_{PD}\right|, \quad (14)$$

where $V_F = 3.3\ V$ is the input and output saturation voltage level in the AN23E04 development board, and $V_{ss} = 12\ V$ is the bias voltage for all op-amps in Figure 6. Here, $K_{pm} = K_{ps} = K_p$, and $K_{dm} = K_{ds} = K_d$.

5.1.2 Constraints in the Haptic Teleoperation Controller Design for Two Robots. There are additional constraints in terms of designing circuits in Figure 5 and Figure 6 that are imposed when using a DC motor as a haptic master device and another DC motor as the slave robot. Typically, the master robot is force (current) controlled while the slave robot is position controlled. Thus, the following considerations apply to Figures 5 and 6, respectively.

- *Large Force Reflection by the Master*: For the DC motor acting as the master, a specific maximum producible torque should be ensured. This will ensure the ability to recreate the feeling of hard-contact tasks for the human operator manipulating the master. Knowing the motor torque constant K and the gear ratio K_g, this results in a specific peak being required for the motor current. This means that, in Figure 6, V_{ref} will need to go as high as a certain value (determined in the Current Control Loop) without violating its constraints for op-amp saturation protection and motor overload protection. If this peak torque is insufficient for doing a certain task, the gear ratio must be increased.
- *Slave Robot Accurate Position Control*: For the slave robot, the position control in Figure 6 has a gain from the input $V_s - V_m$ to the output V_{ref} that may need to be bigger than a certain value for the task to be feasible (e.g., for tasks involving precise positioning and, therefore, high control gains). This gain can be calculated from (13) and (14) as

$$\frac{|V_s - V_m|}{|V_{ref}|} = \frac{R_4}{R_5} \cdot \frac{1}{K_p + sK_d}. \tag{15}$$

These constraints and conditions will be considered during the design procedure below.

5.2 Design Procedure for Controllers in a Teleoperation System

In this section, the above constraints will be applied to our experimental setup in Figure 3 and we will provide design guidelines to systematically satisfy them. The complete design flow chart is presented in Figure 7.

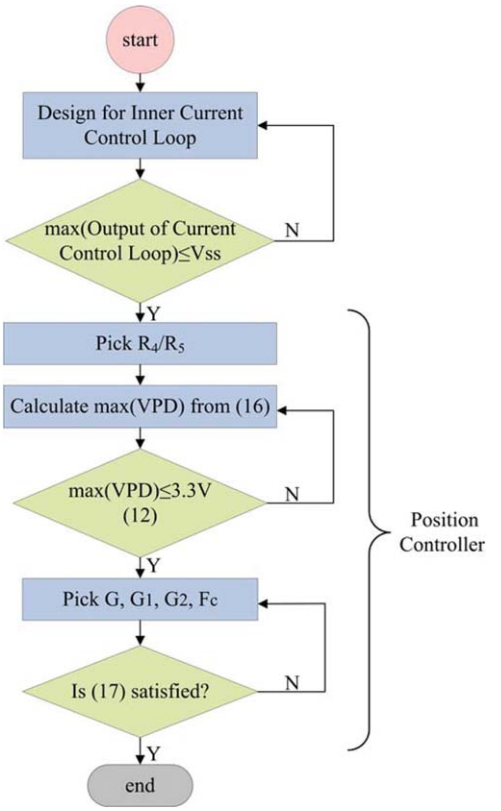

Figure 7. *Flow chart for the control design procedure.*

In the current control loop, Figures 5 and 6, the bias voltage is V_{ss} and V_F, where the latter is the input/output saturation voltage in the FPAA development board. First we need to check the output of the inner Current Control Loop is less than its bias voltage V_{ss}. Then, according to (14),

$$|V_{PD}| \leq \left| \frac{R_4}{R_5} \max(V_{ref}) \right| \tag{16}$$

needs to be satisfied. If $\max(V_{PD}) \leq V_F$, the ratio of $\frac{R_4}{R_5}$ picked is appropriate in (16), otherwise they need to be reselected until the inequality condition is satisfied. Combining with (13) and (15), we can obtain the following condition:

$$\begin{aligned} |V_s - V_m| &= \frac{R_4}{R_5} \cdot \frac{|V_{ref}|}{K_p + s \cdot K_d} \\ &= \frac{|V_{PD}|}{K_p + s \cdot K_d} \leq \frac{\max(V_{PD})}{K_p + s \cdot K_d}. \end{aligned} \tag{17}$$

As the value of V_{PD} has been upper bounded, by picking the proper ratio of $\frac{1}{K_p+s\cdot K_d}$ in (17), it can be ensured that the difference in the initial positions of the master and slave robots (or transient position errors) do not cause op-amp saturation.

5.3 Case Study: Design of FPAA-Based Position Controllers

This section shows the empirical choices of analog components made in the design procedure mentioned above. As mentioned before, we detail only to the design of the outer position controller in Figures 5 and 6. The empirical design of the inner current control loop in Figure 4 can be carried out in a similar way.

In Figure 6, $V_{ss} = 12\ V$ and, for the FPAA board, the saturation voltage is $V_F = 3.3\ V$. We can ensure $|\max(V_{ref})| \leq 7.1\ V$ by considering the saturation conditions and the values of the parameters in the current control loop. Thus, (16) can turn into

$$\begin{aligned} |V_{PD}| &= \left|\left(K_p + s\cdot K_d\right)(V_s - V_m)\right| \\ &\leq \frac{R_4}{R_5} \times 7.1\ V \leq 3.3\ V, \end{aligned} \tag{18}$$

or, alternatively, to

$$\begin{cases} |V_s - V_m| \leq \frac{R_4}{R_5} \times \frac{1}{K_p+s\cdot K_d} \times 7.1\ V \\ |V_s - V_m| \leq \frac{1}{K_p+s\cdot K_d} \times 3.3\ V \\ \frac{R_4}{R_5} \leq \frac{3.3\ V}{7.1\ V} \end{cases} . \tag{19}$$

The maximum difference between the master and slave positions (potentiometer voltages) happens when the two robots are at the opposite and extreme ends of their workspaces. Therefore, the maximum of $|V_s - V_m|$ can be found empirically and used in (19) to properly choose K_p, K_d, which can be chosen quickly by changing parameters inside the FPAA. Note that because of closed-loop control, the actual upper bound on $|V_s - V_m|$ may be much smaller, allowing more relaxed choices for the components in (19).

Another consideration is whether the output force can satisfy the task requirements. The gear ratio for the Servo SRV-02 motor is $K_g = 5 \times 14 = 70$. With the motor torque constant of $K = 0.00767\ Nm/A$, the maximum torque is $T_{\max} = 70 \times 0.00767 \times I_{\max} = 1.2\ Nm$. With $L = 12$ cm being the length of the bar attached to each of the master and slave motors' shafts, the maximum output force of the motors will be $F_{\max} = T_{\max}/L = 10\ N$. This is acceptable because human operators normally perform manipulation tasks with forces in the range of $2\,N \sim 10\,N$, which means this teleoperation system can be used to perform tasks normally performed by humans.

6 Experimental Evaluation of Teleoperation System Transparency

In this section, the maximum stable control gains for two different controllers are tested and compared when a human operates the master robot and the slave robot moves in free space. Next, the position profiles of the two teleoperation systems in hard contact conditions are compared. Then, the hybrid parameters of the two teleoperation systems are compared.

In our experiments, (9) is used as the stability condition. If the master's and/or the slave's positions become unbounded or oscillate indefinitely, the teleoperation system is judged to be unstable. As explained in Section 3.3, larger control gains are expected to increase the transparency of the teleoperation system. This includes lowering the position error between the master and the slave. The smallest sampling period (i.e., the largest sampling rate) achievable in our system is 1 ms, which is used in the following experiments.

6.1 Performance Comparison between Discrete-Time and FPAA-Based Control in Free Motion Conditions

6.1.1 Performance of Discrete-Time Control. For the discrete-time teleoperation, with a fixed small sampling period of $T = 1$-ms, the master/slave position tracking performance under various controller gains that satisfy the stability condition (9) is tested. Since (9) imposes an upper bound of 20 on the control gain for stability reasons, Figure 8 shows the master-slave position tracking results for control gains of

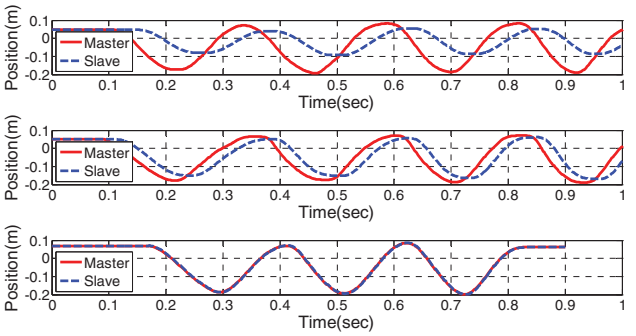

Figure 8. *Master–slave position tracking profiles in discrete-time controlled teleoperation when the operator moves the master and the slave is in free space. The proportional controller gains are $C = 1.0$, $C = 10$, and $C = 20$ for (a), (b), and (c), respectively. The Euclidean norms of the position tracking errors are 0.7886, 0.5625, and 0.0189, respectively.*

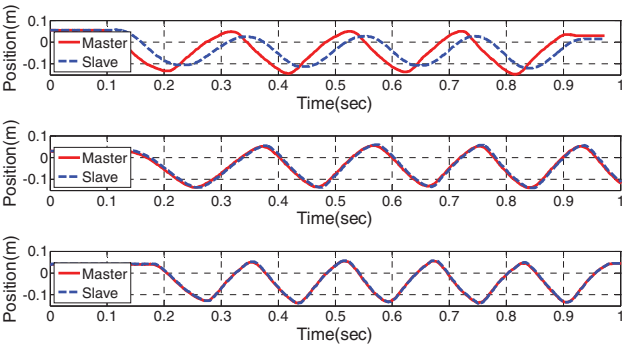

Figure 9. *Master–slave position tracking profiles in continuous-time teleoperation when the operator moves the master and the slave is in free space. The proportional controller gains are $C = 1.0$, $C = 20$, and $C = 80$ for (a), (b), and (c), respectively. The Euclidean norms of the position tracking errors are 0.7917, 0.0242, and 0.0104, respectively.*

1, 10, and 20. When $K > 20$, the system is theoretically outside of the stable region specified by (9), and experimentally the system becomes unstable as well.

6.1.2 Performance of FPAA-Based Control.

With the teleoperation controller also implemented using analog electronic components, various controller gains in the FPAA-based system are tested in order to show the relationship between the control gain and position error. Figure 9 shows the master–slave position tracking results for control gains of 1.0, 20, and 80. While in theory there is no upper bound on the control gain for stability when the teleoperation controllers are implemented in the continuous time, in practice there is a maximum value for the gain due to op-amp saturation inside the FPAA circuit.

It can be seen from Figures 8 and 9 that in both the FPAA-based haptic teleoperation system and the discrete-time teleoperation system, larger control gains always correspond to smaller position tracking errors. Having said that, during the free motion experiment, both the FPAA-based teleoperation system and the discrete-time system can still have satisfactory position tracking using gains lower than the maximum admissible gain. This is not the case, however, in hard contact conditions described next.

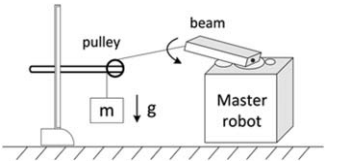

Figure 10. *Achieving repeatable inputs applied to the master robot.*

6.2 Performance Comparison between Discrete-Time and FPAA-Based Control in Hard Contact Conditions

The slave robot can maintain contact with an environment if the human operator applies force on the master robot. To eliminate the influence of the human operator for a fair comparison, the configuration in Figure 10 is used to replace the human operator, where a weight m is connected to the handle of the master robot through a pulley and rope mechanism. Evidently, the "operator" force applied on the master robot is always the same across different experiments. In this way, it is possible to do a fair comparison of system performance between discrete-time versus FPAA-based control.

Figure 11 shows the master–slave position tracking errors of the two systems for their maximum admissible (i.e., stability-preserving) control gains. It can be seen

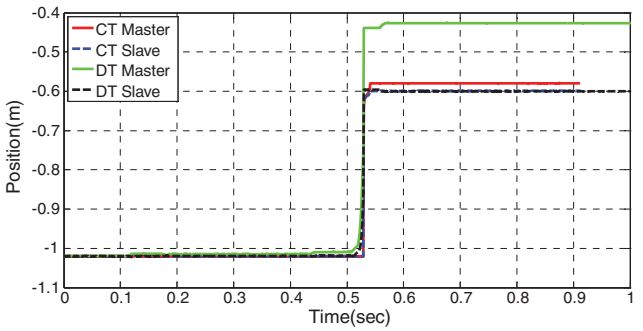

Figure 11. *Position tracking profiles for continuous-time and discrete-time teleoperation when the slave has hit a rigid wall.*

that for the same input force applied on the master robot, the position tracking errors between the master robot and the slave robot are 0.02 and 0.18 under FPAA-based control and discrete-time control, respectively.

Clearly, freeing up the teleoperation system from the sampling-imposed limitations in terms of the control gain upper bound has a significant effect on the system performance.

We can see that the hard contact tasks do need high control gains for accurate position tracking between the master and slave robots. Large position tracking errors also mean large force tracking errors when using PEB teleoperation control; note the position tracking metric h_{21} and the force tracking metric h_{12} in (2) are the same if the master and slave controllers are the same. Also, from a qualitative perspective, in PEB teleoperation control, large position errors when the slave is colliding with a hard object are indicative of inexact force reflection to the user. Later, we will investigate if these also affect actual task success rates. We will observe that small master-slave position tracking errors are sometimes the key to the successful performance of certain tasks such as the one discussed in Section 7.

6.3 Hybrid Parameters Comparisons between Discrete-Time and FPAA-Based Controlled Teleoperation Systems

To further evaluate the transparency differences between the discrete-time controlled and the FPAA-based teleoperation systems, we use the hybrid representation given by (2) and (3) to obtain

$$\begin{aligned} F_h &= h_{11} \cdot sX_m + h_{12} \cdot F_e, \\ -sX_s &= h_{21} \cdot sX_m + h_{22} \cdot F_e. \end{aligned} \tag{20}$$

Each element of the H matrix has a physical meaning. The hybrid parameter $h_{11} = F_h/sX_m|_{F_e=0}$ is the input impedance felt by the operator when the slave is in free motion. The parameter $h_{12} = F_h/F_e|_{sX_m=0}$ is a measure of force tracking in the haptic teleoperation system when the master is locked in place. The parameter $h_{21} = -X_s/X_m|_{F_e=0}$ is a measure of the position (velocity) tracking performance when the slave is in free motion. The parameter $h_{22} = -sX_s/F_e|_{sX_m=0}$ is the output admittance when the master is locked in place. Equation 5 gives the hybrid parameter values for perfect transparency. Nonzero values for h_{11} mean that even when the slave is in free space, the user will receive some force feedback. Nonzero values for h_{22} mean that when the master is locked in place, the slave will move in reaction to slave/environment contact forces. Deviations from 1 and -1 for h_{12} and h_{21} indicate imperfect force tracking and position tracking between the master and slave robots, respectively.

In the experiments in this article, the movement of the master and the slave happen in one rotational degree of freedom. The friction model in the master robot was determined and compensated for. Two different kinds of tests were performed to find the hybrid parameters. First, in free-motion tests, a human operator moves the master robot back and forth for about 1 minute while the slave robot moves in free space. Since $F_e = 0$, the frequency responses $h_{11} = F_h/sX_m$ and $h_{21} = -X_s/X_m$ can be found by applying spectral analysis (MATLAB function *spa*) on the free-motion test data. Second, tests are done by fixing the master robot to a wall while trying to move the slave robot by applying forces on it. Since $X_m = 0$, the frequency responses $h_{12} = F_h/F_e$ and $h_{22} = -sX_s/F_e$ can be found. In the above two tests, the force data concerning external interactions of master robot and slave robots are recorded by two JR3 force sensors (JR3 Inc., Woodland, CA, USA).

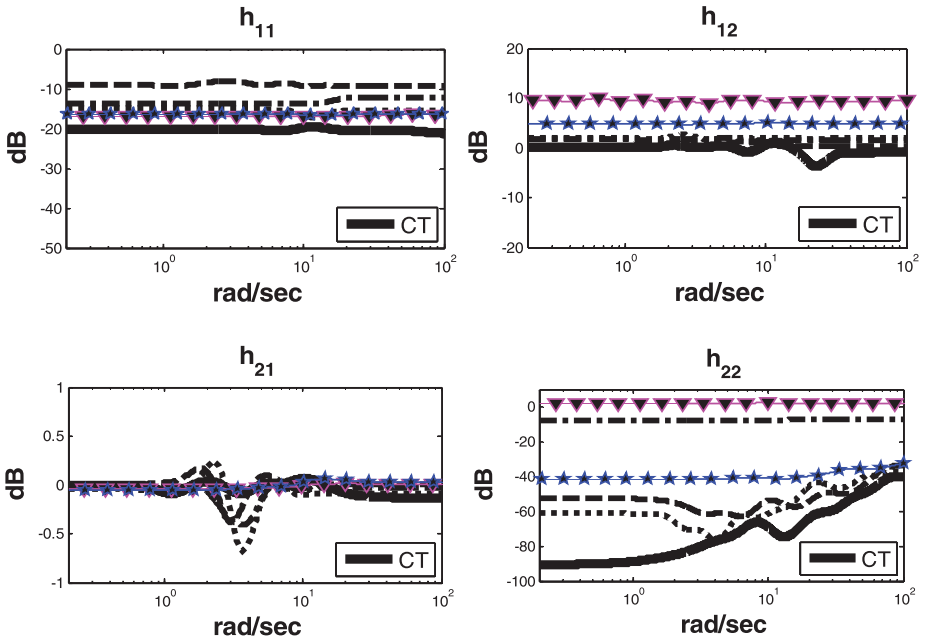

Figure 12. *Magnitudes of the hybrid parameters of the teleoperation systems.*

In the experiments to find the hybrid matrix model, the largest control stabilizing gains for the two teleoperation systems as obtained from Figures 8(c) and 9(c) were used. This is a gain of 20 for the discrete-time controlled system with a 1-ms sampling period, and a gain of 80 for the continuous-time controlled system.

The magnitudes of the experimentally obtained hybrid parameters of the two teleoperation systems are shown in Figure 12. As can be seen, the continuous-time controlled teleoperation system shows its superiority in terms of transparent performance considering the ideal transparency requirement in (5).

In Figure 12, the solid bold line corresponds to the FPAA-based teleoperation system. All others are discrete-time controlled system with different control gains and sampling times: (dash-dot) is with a control gain of 20 for both robots and a 1-ms sampling period; (dotted) control gain is with a control gain of 15 for both robots and a 1-ms sampling period; (dashed) is with control gains of 20 for the master robot and 30 for the slave robot with a 1-ms sampling period; (starred) is with a control gain of 20 for both robots and a 1-ms sampling period; (triangle) is with control gains of 20 for the master robot and 30 for the slave robot and a 1-ms sampling period.

The relatively high value of h_{11} for the discrete-time controlled system is evidence of the fact that the system gives a "sticky" feel of free-motion movements to the operator; the feeling of the free-motion condition will be more realistic under continuous-time control. The better force tracking performance of the continuous-time teleoperation system, that is, $h_{12} \approx 0$ dB, is evident as well. With regard to h_{21}, all spectra are close to 0 dB, indicating both kinds of systems can ensure good position tracking in free space; this is in agreement with the result in Figures 8(c) and 9(c). With regard to h_{22}, somewhat better performance is observed for the FPAA-controlled teleoperation system. Overall, these results demonstrate that an FPAA-based controller can significantly increase the system performance without sacrificing the stability compared to its discrete-time counterpart.

7 Case Study: Object Stiffness Discrimination Task

7.1 Method

In order to compare the system's impedance reflection performance between the discrete-time controlled and the FPAA-based controlled bilateral teleoperations, experiments were conducted in which the task is to discriminate between objects with two different stiffnesses (harder and softer) through bilateral teleoperation system.

This has applications in many domains such as tissue palpation for localizing cancerous tissue in medicine. This task involves a condition similar to the hard contact condition ($Z_e \to \infty$) when the slave robot is in contact with the harder object, and it will be important to ensure $Z_{to}/Z_e \approx 1$, where Z_{to} is the impedance perceived by the human operator, for successful stiffness discrimination. Evidently, for this task, successful user task performance (high Z_{to}) goes hand in hand with high system transparency as it was discussed in Section 3.1. In the absence of good system transparency, the difference between the impedances perceived by the human operator for the two objects will not be sufficient to lead to successful object stiffness discrimination.

7.1.1 Participants. A total of 30 people (15 males and 15 females) participated in our experiments. The participants had little to average exposure to haptics and average experience with the bilateral teleoperation system. The participants' primary goal was defined as distinguishing objects in terms of their relative stiffness without visual and audio feedback. All the participants volunteered for the experiment and gave their informed consent.

7.1.2 Materials. The master–slave setup used in this experiment is shown in Figure 13. Based on the setup shown in Figure 3, two identical Servo SRV-02 Quick Connect Modules (Quanser Inc., Markham, ON, Canada) are the revolute-joint master and slave robots. The hard object is a block of wood, and the volume of the wood is 15 cm × 15 cm × 4 cm, which density is about $0.44 \sim 0.57\,\mathrm{g/cm^3}$. The second softer

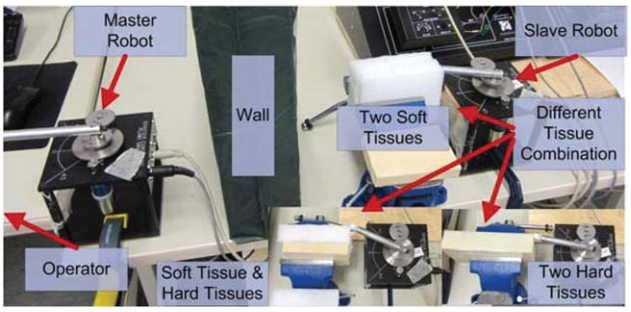

Figure 13. *Master–slave setup for performing the telemanipulated object stiffness discrimination task.*

object is a block of compressed packaging foam, and the volume of the foam is 20 cm × 15 cm × 5 cm, with a density of about $0.10 \sim 0.14\,\mathrm{g/cm^3}$. Both objects have high stiffnesses with a small difference between the two (the wood is closer to $Z_e \to \infty$). Before the experiments, each participant was given the mentioned wood and compressed packaging foam to feel the difference by fingers. The feedback is consistent: the wood feels harder than the foam, yet the difference is not obvious when only felt by human fingers. The purpose of the experiment is to see whether the teleoperated control systems can help participants identify objects' stiffness, the difference of which is not obvious through touching by human fingers; thus the material chosen is appropriate.

7.1.3 Procedure. In each trial, one out of the three different controller (FPAA-based controller, discrete-time controller with a 1-ms sampling period, and discrete-time controller with a 10-ms sampling period) and a combination of two objects samples (the hard and soft objects or the same object twice) were presented to the operator. In total, nine different conditions were presented in a randomized order to each operator.

Each participant performed three trials (27 times) with a short break between them. The trials also were presented in a randomized order to each operator.

Before the experiments, each participant was given two to three practice trials until he or she felt comfortable with the operation of the master–slave system and

understood the task. The participants were told that they had 30 seconds to finish the task, which was found to be enough time.

After an object was presented through the teleoperation system to a participant and probed, it was replaced with a different or the same object. After probing the second sample again through the teleoperation system, the participant had to declare if the first object was harder than the second object or softer than it, or if the two objects had the same stiffness.

7.2 Results

The final results, averaged over the 27 time experiments under 9 different conditions for each participant, are presented graphically in Figure 14. In Figure 14, each bar represents the mean percentage under corresponding control conditions, and every standard error of mean is shown to demonstrate the reliability of statistical inference. The cases 1 to 3 correspond to FPAA-based teleoperation. The cases 4 to 6 correspond to the teleoperation system with discrete-time controller and 1-ms sampling time. The cases 7 to 9 correspond to teleoperation system with discrete-time controller and 10-ms sampling time. In cases 1, 4, and 7, the softer object was presented twice to the operator. In cases 2, 5, and 8, the harder object was presented twice to the operator. In cases 3, 6, and 9, two objects with different stiffnesses were presented to the operator randomly.

As can be seen, the success rate in FPAA-based controlled teleoperation system is the highest. According to the feedback from operators, they can always feel a stronger force feedback with the FPAA-based controller than with the discrete-time controller. Under discrete-time control, the harder object feels like the softer one, thus explaining for zero success rates in cases 5 and 8. Every standard error of mean is small enough to show the result is reliable under most circumstances.

In order to analyze the statistical significance of the results shown in Figure 14, a right-tailed t-test between different pairs of controllers is used for further investigation. The significant difference threshold here chosen is 0.05, when $p \leq 0.05$ the two samples compared have

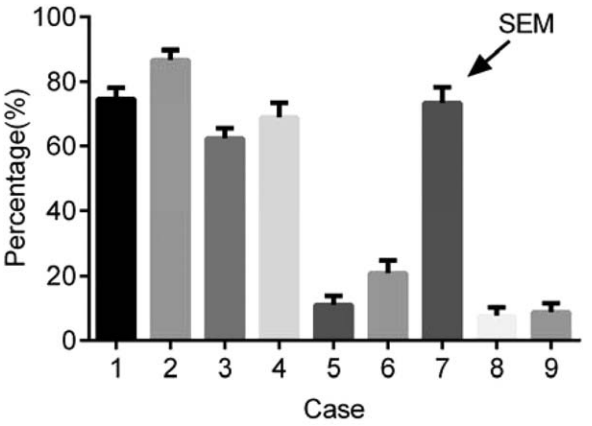

Figure 14. *Success rates of the task under different control conditions.*

significant difference, otherwise, the difference is not remarkable.

The p-value for the t-test between 1 and 4 is $p = 0.1525$, which is bigger than the selected threshold value of statistical significance (0.05). The same can be said about cases 1 and 7 with $p = 0.4158$, implying that there exists no statistical difference among the three different controllers when probing the softer object twice—all controllers manage to give sufficient feeling to the participants to perform the task with high success rates. The p-value of 2 versus 5 and 2 versus 8 are $p = 0.0151 \times e^{-17}$ and $p = 0.1970 \times e^{-17}$ respectively, indicating the statistical significance of higher success rates for FPAA-based controller compared to discrete-time controller when probing the harder object twice. The other two right-tailed t-tests between 3 and 6 ($p = 0.1742 \times e^{-8}$), and between 3 and 9 ($p = 0.0645 \times e^{-12}$) also confirm the existence of significant differences between the corresponding pairs, indicating directly the better performance of the FPAA-based controller in distinguishing different stiffnesses. Overall, the task success rate is much higher in FPAA-based teleoperation than in discrete-time controlled teleoperation even for a small sampling period (1 ms) and the performance gap widens as the sampling period increases (10 ms) when dealing with harder stiffness objects.

7.3 Discussion

It can be observed from the results that both the discrete-time controlled and the FPAA-based controlled teleoperation system can accomplish the probing task with the softer object; however, large errors can be introduced when dealing with the harder object. The worse performance happens when the sampling time of digital control increases. The FPAA-based controlled teleoperation system is much better in transmitting task-related information (transmitted impedance) than the discrete-time controlled teleoperation system, especially as the sampling period increased.

8 Conclusions and Future Work

In this article, the performance of an FPAA-based controlled bilateral teleoperation system was contrasted to that of a discrete-time controlled teleoperation system in theory and experiments. The work showed that an FPAA-based controller can outperform discrete-time controllers in terms of hybrid parameters performance and task success rates by widening the *Z*-width of the system.

There are some limitations for the FPAA-based controller that need to be considered in future work. First of all, although the proposed controller can provide higher PD control gain for teleoperation system and satisfy the task performance requirement in this article while simplifying the analog design process, the main defect of an analog controller still exists, which is that it cannot realize complicated mathematical algorithm when needed.

So one possible extension of the current study includes mixing the capabilities of analog and digital controllers to achieve highly transparent and stable teleoperation in haptic applications involving both soft and hard environments or both force and position control, which can program complex algorithm while keeping the analog advantage.

This article focuses on the task performance and task success rates, both of which need only the best combination of all related parameters (stiffness, damping coefficients, control gains, etc.); thus the stiffness parameters are fixed in the experiment. This consideration leads to the second limitation of the proposed control method, which is that the stiffness chosen in the experiment is fixed, once it has been chosen from the best result of several prior tests. As one advantage of applying FPAA, it can realize the dynamic parameter changes during the experiment and show more flexibility of the controller in bilateral teleoperation system, which can be a second extension of our work.

Acknowledgments

This research was supported by the Natural Sciences and Engineering Research Council (NSERC) of Canada, by the Canada Foundation for Innovation (CFI), by Self-Planned Task (NO.SKLRS201403B) of State Key Laboratory of Robotics and System (HIT), and by the China Scholarship Council (CSC) under grant [2013]06120200.

References

Aliaga, M., Rubio, A., & Sanchez, E. (2004). Experimental quantitative comparison of different control architectures for master–slave teleoperation. *IEEE Transactions on Control Systems Technology, 12*, 2–11.

Anadigm Inc. (2004). *AnadigmDesigner@2 user manual.* Mesa, AZ.

Ashrafzadeh, A. (2007). Power management: Analog control vs. digital. Retrieved from http://www.eetimes.com/document.asp?doc_id=1271501

Aziminejad, A., Tavakoli, M., Patel, R. V., & Moallem, M. (2008). Stability and performance in delayed bilateral teleoperation: Theory and experiments. *Control Engineering Practice, 16*, 1329–1343.

Bratt, A. (1998). Motorola field programmable analogue arrays, present hardware and future trends. *Proceedings of IEEE Half-Day Colloquium on Evolvable Hardware Systems, 1988/233*, 1/1–1/5.

Brezovich, I. A. (2011). *Digital vs. analogue control systems.* Paper presented at The 2011 Annual Meeting of the American College of Medical Physics.

Chang, P. H., & Kim, J. (2012). Telepresence index for bilateral teleoperations. *IEEE Transactions on Systems, Man, and Cybernetics, Part B: Cybernetics, 42*(1), 81–92.

Colgate, J. E., & Schenkel, G. G. (1997). Passivity of a class of sampled-data systems: Application to haptic interfaces. *Journal of Robotic Systems, 14*, 37–47.

Colgate, J. E., & Brown, J. M. (1994). Factors affecting the Z-width of a haptic display. *Proceedings of the IEEE 1994 International Conference on Robotics and Automation*, 3205–3210.

Courtecuisse, H., Jung, H., Allard, J., Duriez, C., Lee, D. Y., & Cotin, S. (2010). GPU-based real-time soft tissue deformation with cutting and haptic feedback. *Progress in Biophysics & Molecular Biology, 103*, 159–168.

Cypress Semiconductor Corp. (2014). CY8C29466/CY8C29566/CY8C29666/CY8C29866: PSoCR Programmable System-on-Chip™. San Jose, CA.

Diolaiti, N., Niemeyer, G., Barbagli, F., & Salisbury, J. K. (2006). Stability of haptic rendering: Discretization, quantization, time delay, and Coulomb effects. *IEEE Transactions on Robotics, 22*, 256–268.

Haykin, S. S. (1970). *Active network theory*. Reading, MA.: Addison-Wesley.

Hewitson, M. (2010). *Digital vs. analog control*. Paper presented at the GEO ISC Meeting.

Jazayeri, A., & Tavakoli, M. (2010). Stability analysis of sampled-data teleoperation systems. *49th IEEE Conference on Decision and Control*, 6.

Jazayeri, A., & Tavakoli, M. (2012). *Revisiting Llewellyn's absolute stability criterion for bilateral teleoperation systems under non-passive operator or environment*. Paper presented at the 2012 IEEE/RSJ International Conference on Intelligent Robots and Systems.

Jazayeri, A., & Tavakoli, M. (2013). Absolute stability analysis of sampled-data scaled bilateral teleoperation systems. *Control Engineering Practice, 21*, 1053–1064.

Khabbaz, F. H., Goldenberg, A., & Drake, J. (2016). Force discrimination ability of the human hand near absolute threshold for the design of force feedback systems in teleoperations. *Presence: Teleoperators and Virtual Environments, 25*(1), 47–60.

Lathan, C. E., & Tracey, M. (2002). The effects of operator spatial perception and sensory feedback on human-robot teleoperation performance. *Presence: Teleoperators and Virtual Environments, 11*(4), 368–377.

Lee, D. J., & Spong, M. W. (2006). Passive bilateral teleoperation with constant time delay. *IEEE Transactions on Robotics, 22*, 269–281.

Li, J., Tavakoli, M., Mendez, V., & Huang, Q. (2013). *Conservatism of passivity criteria for stability analysis of trilateral haptic systems*. Paper presented at the 2013 World Haptics Conference.

Liu, C. J., Chen, Q. J., & Wang, D. W. (2011). CPG-inspired workspace trajectory generation and adaptive locomotion control for quadruped robots. *IEEE Transactions on Systems, Man, and Cybernetics, Part B: Cybernetics, 41*(3), 867–880.

Llewellyn, F. B. (1952). Some fundamental properties of transmission systems. *Proceedings of the Institute of Radio Engineers, 40*, 271–283.

Malcher, A., & Falkowski, P. (2014). Analog reconfigurable circuits. *International Journal of Electronics and Telecommunications, 60*(1), 15–26.

Mafi, R., Sirouspour, S., Mahdavikhah, B., Moody, B., Elizeh, K., & Kinsman, A. B. (2010). A parallel computing platform for real-time haptic interaction with deformable bodies. *IEEE Transactions on Haptics, 3*, 211–223.

Ogata, K. (1995). *Discrete-time control systems* (2nd ed.). New York: Prentice Hall.

Ramsden, E. (2001). The ispPAC family of reconfigurable analog circuits. *Proceedings of the Third NASA/DoD Workshop on Evolvable Hardware*, 176–181.

Sheridan, T. (1993). A historical teleoperation. *Presence: Teleoperators and Virtual Environments, 2*(3), 259–259.

Spinner, T., Srinivasan, B., & Rengaswamy, R. (2014). Data-based automated diagnosis and iterative retuning of Proportional-Integral (PI) controllers. *Control Engineering Practice, 29*, 23–41.

Tavakoli, M., & Aziminejad, A. (2007). High-fidelity bilateral teleoperation systems and the effect of multimodal haptics. *IEEE Transaction on Systems, Man, and Cybernetics, Part B: Cybernetics, 37*(6), 1512–1528.

Zetex Semiconductors Ltd. (1999). Totally reconfigurable analog circuit: TRAC. Oldham, UK.

Appendix

In Figures 1 and 2, the continuous-time models of the human operator and the environment are:

$$\begin{aligned} \tilde{F}_h - F_h &= Z_h(s)sX_m, \\ \tilde{F}_e - F_e &= Z_e(s)sX_s, \end{aligned} \tag{21}$$

where s is the Laplace operator.

The continuous-time dynamics of the master and slave robots in the s-domain are:

$$\begin{aligned} sX_m &= Z_m(-F_m + F_h), \\ sX_s &= Z_s(-F_s + F_e), \end{aligned} \tag{22}$$

where F_m and F_s are the control signals for the master and the slave, respectively. Z_m, Z_s represent impedances of the master and slave robots and are considered to be:

$$Z_m = \frac{1}{m_m s + b_m}, \quad Z_s = \frac{1}{m_s s + b_s}, \tag{23}$$

where m_m and m_s denote the masses of the master and slave robots, and b_m and b_s denote the corresponding damping terms.

For the discrete-time controller designed as in Figure 2, the sampled-data outputs of the master and slave controllers are (Jazayeri & Tavakoli, 2010):

$$F_m^*(s) = C_m(z)[X_s^*(s) - n_p X_m^*(s)], \quad F_s^*(s) = C_s(z)[n_p X_m^*(s) - X_s^*(s)], \tag{24}$$

where * shows sampled signals, and n_p defines the position ratio between the master and slave robots.